NISTIR 6299

A Heat Transfer Model for Fire Fighter's Protective Clothing

William E. Mell
J. Randall Lawson

United States Department of Commerce
National Institute of Standards and Technology

NISTIR 6299

A Heat Transfer Model for Fire Fighter's Protective Clothing

William E. Mell
J. Randall Lawson

January 1999

U.S. Department of Commerce
William M. Daley, *Secretary*
National Institute of Standards and Technology
Raymond G. Kammer, *Director*

U.S. Fire Administration
Carrye Brown, *Administrator*
16825 South Seton Avenue
Emmitsburg, Maryland 21727

Contents

List of Figures

List of Tables

Nomenclature

c_p	[J/K·kg] specific heat
d	[m] thickness of a material layer
d_a	[m] thickness of air layer
e	interface between control volumes P and E
D	(m^2/s) diffusivity ($k/\rho c_p$)
E	midpoint of right control volume in finite difference scheme
$E_{b,\lambda}$	[W/(m^2·μm)] spectral blackbody emissive power
$E_{\lambda,l}$	spectral emissive power incident on fabric layer l
g	[W/m^3] internal energy generation rate per unit volume or [m/s^2] gravitational acceleration
h_c	[W/(m^2·K)] surface heat transfer coefficient for convection
Gr	$= 2g(T - T_\infty) L^3 \rho_G^2 / (T_\infty \mu_G^2)$ Grashof number
I	[W/(m^2-μm-sr] radiant intensity
$I_{b,\lambda}$	blackbody spectral intensity
k	[W/K·m] thermal conductivity
k^*	effective conductivity coefficient, used in determining q_{CD} at internal cell interfaces
k_Γ	effective conductivity coefficient, used in determining q_{CD} at gas/solid interfaces
L	[m] streamwise distance to the initiation of natural convection
Nu	Nusselt number
P	midpoint of central control volume in finite difference scheme
Pr	$= \mu_G c_{p,G} / k_G$ Prandtl number
q	[W/m^2] heat flux
q_{CD}	heat flux due to conduction
q_e	external radiation heat flux on left side of the first protective clothing layer (shell layer)
q_R	radiation heat flux
Ra	= Pr |Gr|, Rayleigh number
r	reflectivity of incident thermal radiation
s	[m] pathlength of radiation beam
t	[s] time
T	[K] temperature
T_∞	ambient air temperature
w	interface between control volumes W and P
W	midpoint of left control volume in finite difference scheme
x	[m] distance measure into protective clothing

Greek Symbols

α	absorptivity
β	= cos(θ), cosine of polar angle locating radiation beam in spherical coordinates
δ	Dirac delta function
δ_e, δ_w	distance between midpoints of control volumes *P* and *E*, and *P* and *W*, respectively
δ_e^-	distance from cell interface *e* to point *P* in finite difference scheme
δ_e^+	distance from cell interface *e* to point *E* in finite difference scheme
ε	emissivity
η	nondimensional optical depth variable
θ	polar angle locating radiation beam in spherical coordinates
κ	[1/m] absorbtion (extinction) coefficient
λ	[μm] wavelength of thermal radiation
μ	[kg/(m·s)] dynamic viscosity
ρ	[kg/m^3] mass density
σ	5.6697×10^{-8} W/(m^2·K^4)] Stefan-Boltzmann constant
τ	transmissivity of incident thermal radiation
ϕ	azimuthal angle locating radiation beam in spherical coordinates
$\underline{\hat{\Omega}}$	direction of radiative energy propagation

Subscripts

1, 2 ...	material layer 1, 2, ...
a	air
d	total thickness of air gap or material layer
l	material or fabric layer *l*
G	gas cell
S	solid cell
Γ	gas/solid or solid/solid interface
λ	spectral dependence

Superscripts

+	forward direction
-	backward or reverse direction
i	incident (flux or intensity) on material boundary

BLANK PAGE

A Heat Transfer Model for Fire Fighters' Protective Clothing

by

William E. Mell and J. Randall Lawson

Abstract

An accurate and flexible model of heat transfer through fire fighter protective clothing has many uses. The degree of protection, in terms of burn injury and heat stress, of a particular fabric assembly could be investigated. The expected performance of new or candidate fabric designs or fabric combinations could be analyzed cheaply and quickly.

This paper presents the first stage in the development of a heat transfer model for fire fighters' protective clothing. The protective fabrics are assumed to be dry (e.g., no moisture from perspiration) and the fabric temperatures considered are below the point of thermal degradation (e.g., melting or charring). Many burn injuries to fire fighters occur even when there is no thermal degradation of their protective gear. A planar geometry of the fabric layers is assumed with one-dimensional heat transfer. The forward-reverse model is used for radiative heat transfer. The accuracy of the model is tested by comparing time dependent temperatures from both within and on the surface of a typical fabric assembly to those obtained experimentally. Overall the model performed well, especially in the interior of the garment where the temperature difference between the experiment and simulation was within 5 ˚C. The predicted temperature on the outer shell of the garment differed most from experimental values (by as much as 24 ˚C). This was probably due to the absence of fabric-specific optical properties (transmissivity and reflectivity) used for model input.

Key Words: heat transfer; comuter modeling; fire; fire fighter; fire fighter safety; protective clothing; thermal insulation; turnout coats

1 Introduction

The thermal performance of fire fighters' protective clothing has been a point of interest and discussion for several decades. However, little detailed scientific information is available on the technical issues. Much of these discussions are based on fire service field experience, and many of these studies are difficult to reproduce. Very little has been done to develop methods for predicting the thermal performance of protective clothing throughout the *range* of fire environments normally faced by the fire fighter.

Torvi [1] provides a review of work done on heat and mass transfer models applicable to fabrics in the high heat flux range that a fire fighter may experience. Most of this work dates from the 1960's [2] and 1970's [3-5] when computers were significantly less advanced. The Government-Industry Research Committee on Fabric Flammability considered mainly flammable fabrics used by the ordinary consumer [3], [4]. Morse *et al.* [5] studied heat transfer and burn injury risk from exposure to JP-4 fuel fires. Only three protective clothing materials were examined for use in air force flight suits. Also, some model properties were determined by fitting the model results to experimental data. Stoll and colleagues used a combination of analytical and experimental techniques to measure the thermal response of single fabric layers over skin. They developed diagnostics to rate the protection offered by a fabric with known properties [6-8]. Their work eventually lead to the Thermal Protective Performance (TPP) test [9]. Two recent modeling works are by Bamford and Boydell [10] who developed a finite difference based burn injury evaluation code and Torvi [1] who developed a finite element code to simulate the TPP test.

Two thermal performance tests are in the NFPA1971 [11] standard: a fabric flammability test and the TPP test. These tests, along with the development of new fabrics with improved thermal properties, have led to significant changes in fire fighter clothing. The fabric flammability test has resulted in the development of protective garments that resist flaming ignition. The TPP test has led to the use of protective clothing with better insulating properties. The TTP test was originally designed to test fabric performance under short duration, high heat flux exposures (such as flash fires and JP-4 fuel fires from deck crashes of planes on aircraft carriers). The NFPA standard TPP test method measures heat flow through the garment while exposed to a 84 kW/m^2 (2 $cal/cm^2 \cdot s$) thermal environment. This level of flux is chosen in order to replicate a flash fire or mid-range post-flashover exposure. A single copper calorimeter is used to measure heat transfer through a protective clothing assembly, and no data is gathered on the thermal performance of individual protective clothing components.

A minimum TPP rating of 35 is required according to the NFPA standard. At this level of protection a fire fighter would have approximately 17.5 seconds to escape from a flashover exposure before sustaining second degree burns. Work by Krasny *et al.* [12], however, suggests that fire fighters wearing TPP 35 garments are likely to receive serious burn injuries in less than 10 seconds when exposed to a flashover fire environment. Peacock *et al.* [13] found that the TPP test was best able to predict the *relative* thermal protection of different turn-out gear in room fires which were rapidly developing into flashover.

To date the TPP test is the only source of data relevant to the thermal performance of protective clothing. It is relatively inexpensive to run, but somewhat complicated and only provides the user with thermal performance of the protective garment as a whole. A more informative test method would provide thermal performance measures of the component fabrics and, therefore, heat transfer within the garment. TPP test measurements are also time restricted because of the thermal properties of the copper calorimeter. Gener-

ally, TPP tests on thermal protective clothing have been conducted using time periods less than one minute [11]. Thus, the TPP test does not produce the detailed information necessary for evaluating the thermal performance of protective clothing over a range of conditions. This is an important issue since, many fire fighter burn injuries appear to result from longer duration moderate heat flux exposures [14].

Fire fighters can be burned by radiant heat energy that is produced by a fire or by a combination of radiant energy and localized flame contact exposure as replicated by the TPP test. Some injuries also occur as a result of compressing the protective garment against the skin, either by touching a hot object or by placing tension on the garment fabric until it becomes compressed against the skin. In addition to these mechanisms, moisture in protective clothing can significantly change the garment's protective performance. As stated in NISTIR 5804, garments that are wet may exhibit significantly higher heat transfer rates than garments that are dry [14]. Burn injuries that result from the heating and evaporation of moisture trapped within one's protective clothing is also significant. These injuries are generally referred to as scald or steam burns. Moisture may also help to store heat energy in protective clothing [14].

The Building and Fire Research Laboratory (BFRL) at the National Institute of Standards and Technology (NIST) has been developing two tools to further the understanding and prediction of the thermal performance of fire fighters' protective clothing. One tool is a laboratory test apparatus that exposes specimens of protective clothing to radiant heat from a gas–fired radiant panel and/or flames from a gas pilot line burner. Temperature measurements can be made by placing thermocouples on and within the fabric assembly. This experimental test apparatus, discussed in Sec. 2, was designed to measure the temperature distribution through layers of protective clothing over a range of conditions. It is possible to subject the protective clothing materials or specimen to various levels of incident radiant heat flux and to investigate the effects of compression and moisture. The second tool is the subject of this paper. It is an analytical computer model that provides detailed information on heat transfer through the protective clothing assembly. Among the other models developed to date, this model is most similar to that of Bamford and Boydell [10]. However, development of the model discussed here will occur in stages. The performance of the model will be tested by comparing temperature predictions to measurements from the laboratory test apparatus. Ultimately, a detailed skin model can be included if needed to provide burn injury predictions. When fully developed, this predictive model could be used as an aid in the design of candidate protective clothing systems, evaluating the performance of current protective clothing systems in various thermal environments, and as a tool to study potential issues related to the causes of fire fighter burn injuries. It could also be used as a training tool for fire service personnel.

Next, in Sec. 2, a brief description of the experimental test apparatus is given. The derivation of the heat transfer model is presented in Sec. 3, followed by its numerical implementation, the thermo–physical characteristics of the turnout coat considered here, and model predictions versus experimental results.

2 Experimental Test Apparatus

The test apparatus was designed to evaluate the thermal performance of fire fighters' protective clothing over a wide range of thermal exposures. Results from the test provide a thermocouple-based time history of the temperature at fabric layer surfaces (e.g., the outer or inner surface of a garment assembly or between component layers). In addition, the test method may be used for measuring latent heat or energy

stored in the clothing assembly upon being exposed to a selected thermal environment for a specified period of time. The test apparatus and its components are shown in Figs. 2.1 through 2.3. The specimen holder is mounted on a trolley. This allows the specimen to be easily moved and then secured at different distances from the radiant panel. In this way the radiant flux, due to the radiant panel, incident on the outer surface of the garment specimen can range from about 1.0 kW/m^2 to more than 50 kW/m^2. The test specimen may also be subjected to a pilot flame during any part of a test to evaluate the thermal performance associated with direct flame contact. Test specimens, Fig. 2.4, measure 305 mm x 305 mm (12 in x 12 in) square. The surface of the specimen which is exposed to test conditions, when held in the specimen holder, measures 255 mm x 255 mm (10 in x 10 in). See photograph showing the test specimen prepared for test in Fig. 2.1 and the sketch of the specimen holders in Fig. 2.4. This specimen size was selected to allow for the measurement of protective clothing system assemblies that may have surface features (i.e., trim, pads, patches, or pockets) that require evaluation. Tests may be conducted with either an open back or closed back configuration. Only the open back configuration was used here. The basic locations for thermocouple attachment are shown in Fig. 2.5. A minimum of three thermocouples are required for making heat flow measurements through a garment assembly. These are thermocouples 1, 2, and 3 shown in Fig. 2.5. Thermocouple number 4 is used to measure open field temperatures when a surface attachment is applied to the shell material. Protective clothing specimens may be tested dry or wet so that the effects of moisture can be measured.

In this study the test apparatus was used to help gauge the validity of the heat transfer model developed below. Since this is the first stage in the development of the model conditions were kept simple. Thus, experimental results presented below are for dry specimens in the open back configuration. Also, only the radiant panel was used – there was no direct flame contact.

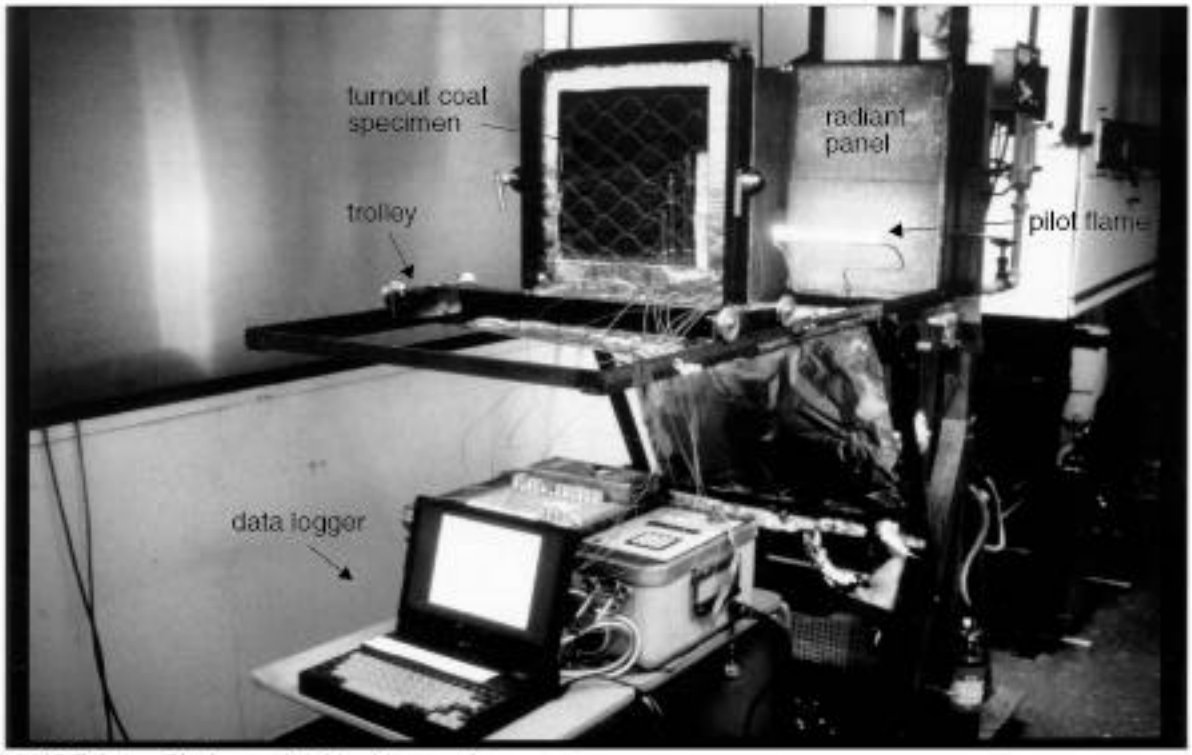

FIGURE 2.1: Photograph of test apparatus.

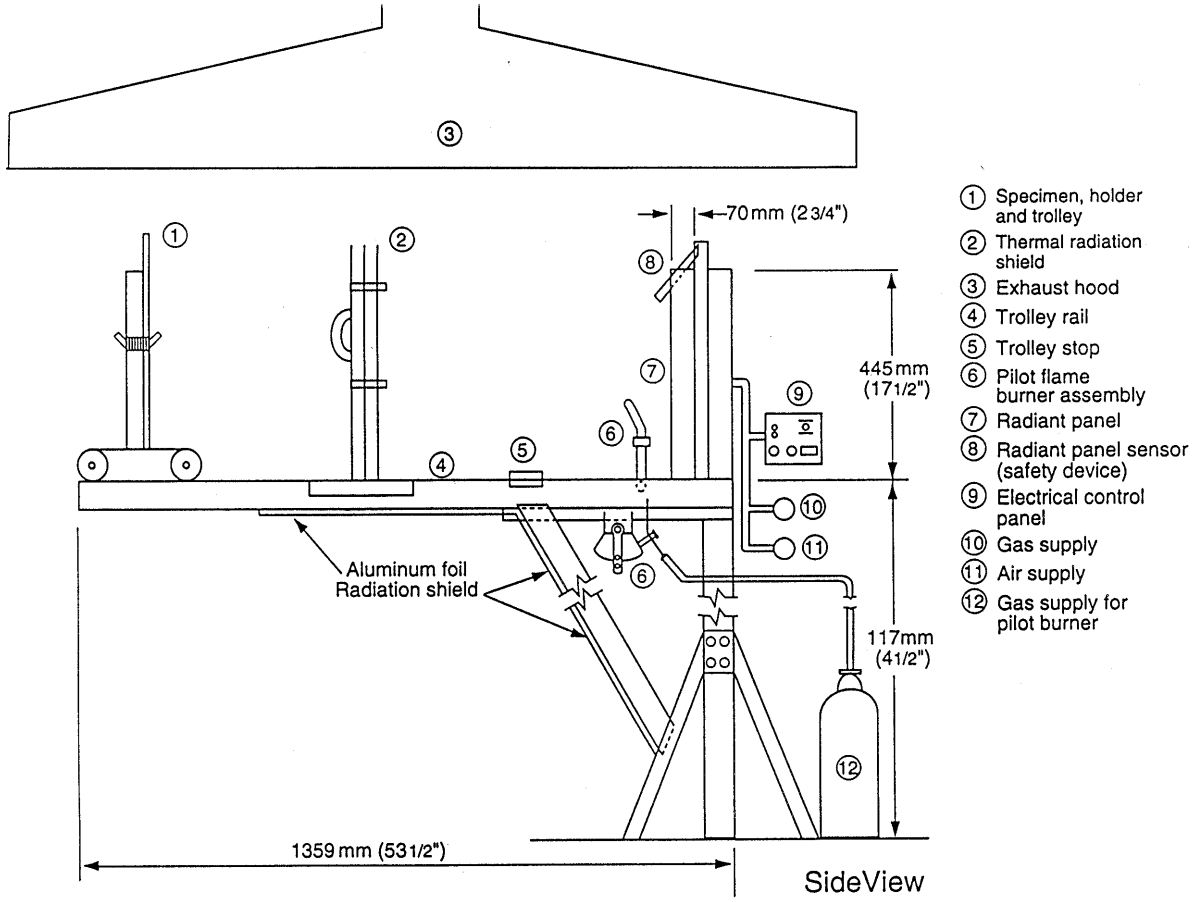

FIGURE 2.2: Sketch of side view of test apparatus.

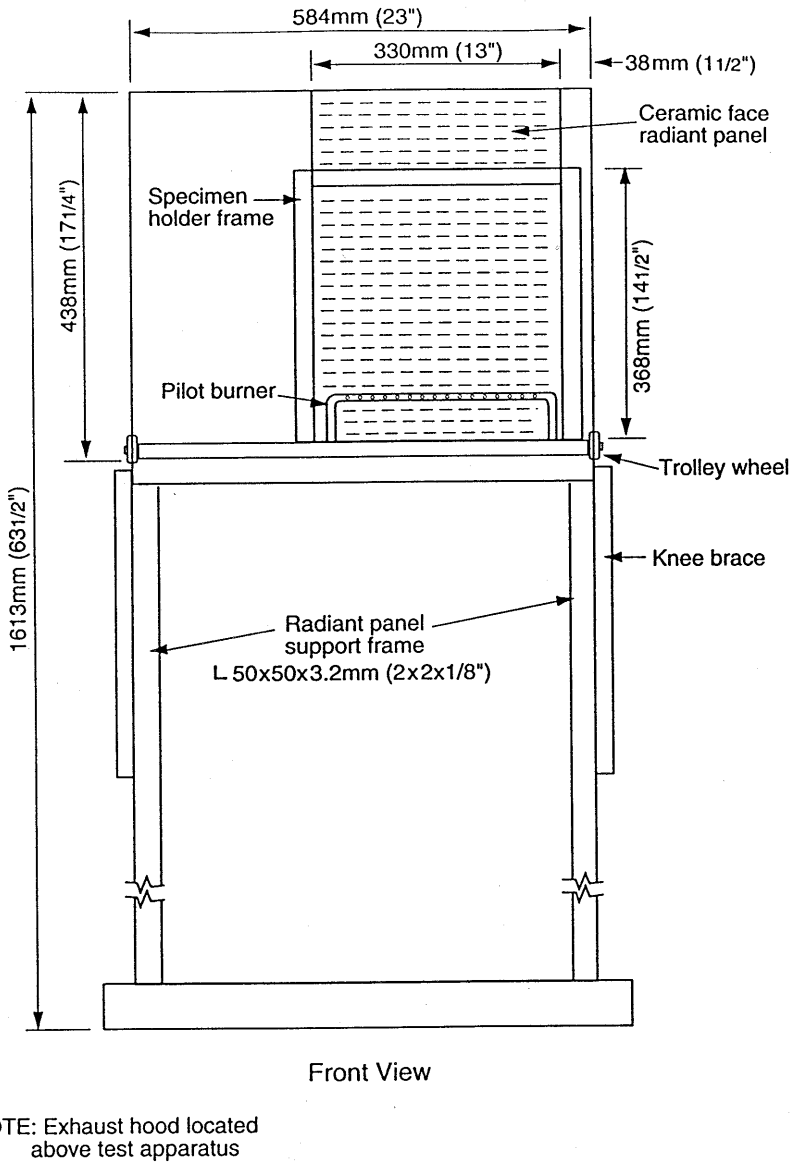

FIGURE 2.3: Sketch of the front view of test apparatus.

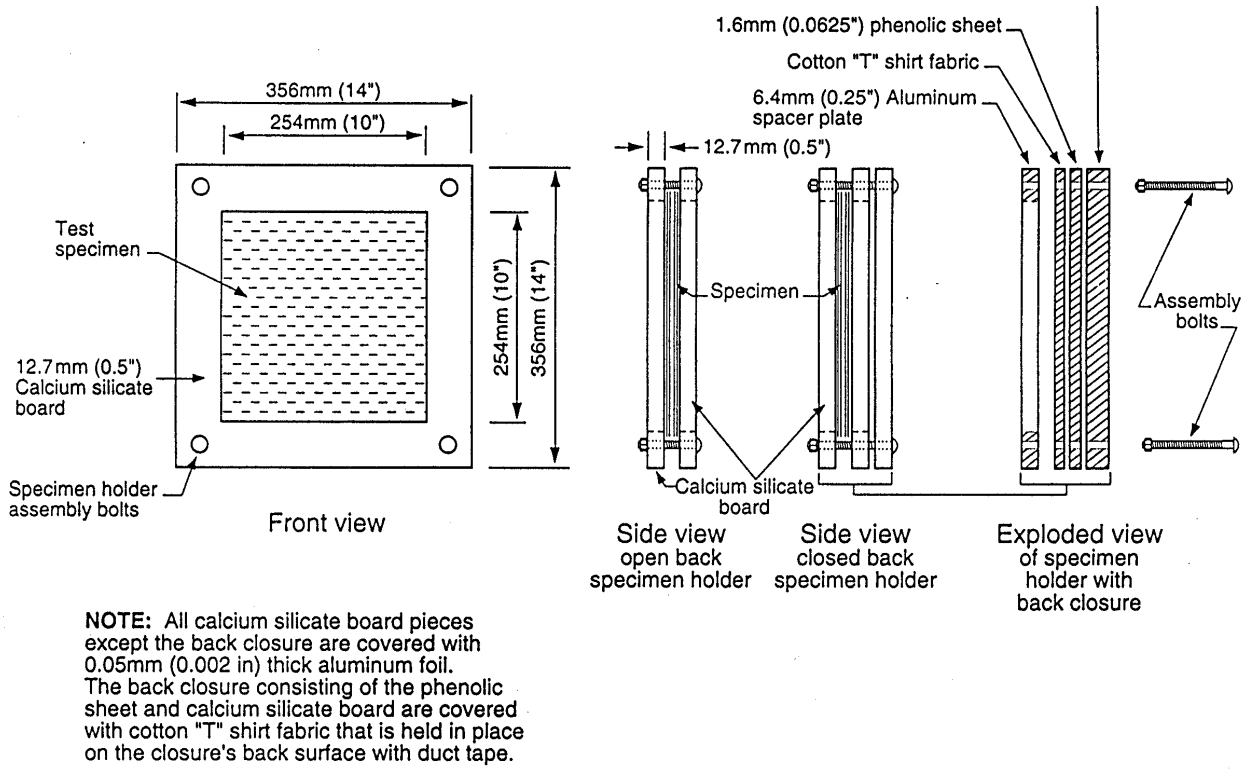

NOTE: All calcium silicate board pieces except the back closure are covered with 0.05mm (0.002 in) thick aluminum foil. The back closure consisting of the phenolic sheet and calcium silicate board are covered with cotton "T" shirt fabric that is held in place on the closure's back surface with duct tape.

FIGURE 2.4: Sketch of open back and closed back specimen holders.

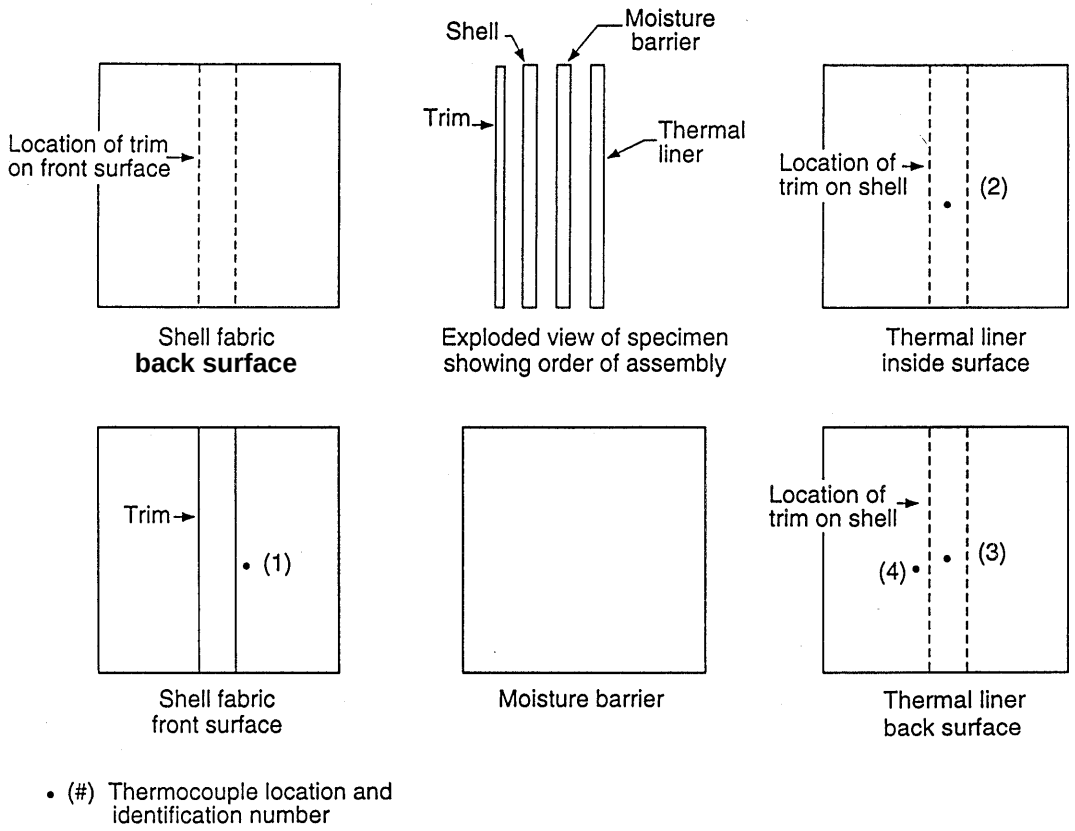

FIGURE 2.5: Normal locations of thermocouples used for testing.

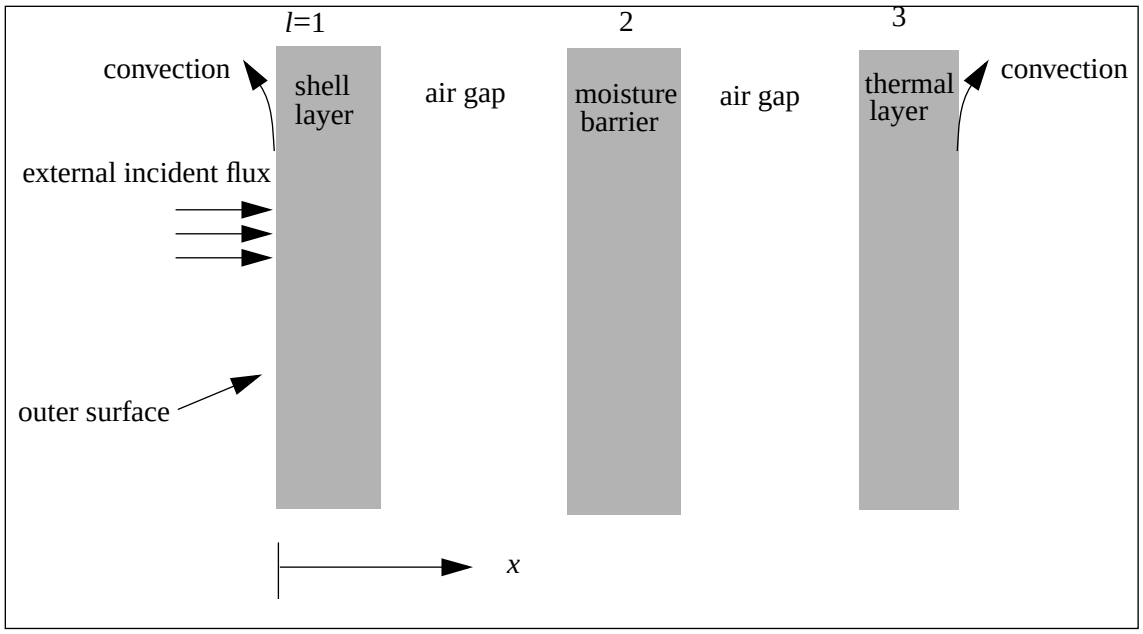

FIGURE 3.1: Schematic cross-section of a three layered firefighter protective clothing ensemble surrounded by ambient air. This scenario mimics that of the experimental test apparatus used to test the model.

3 Heat Transfer Model

This work is the first step in the development of a heat transfer model for protective clothing worn by fire fighters. Heat transfer through fire fighter's clothing, ultimately reaching the skin, is largely due to radiant energy from the surroundings. This process, as opposed to direct contact with flames, is the focus of the current stage of the model. In addition, the influence of moisture is not considered and temperatures are assumed to be too low for melting or gasification of the fabrics (i.e., thermal degradation of the fabric). Many burn injuries to fire fighters occur even when there is little or no thermal degradation of their protective gear. It is hoped that the heat transfer model and the experimental test apparatus discussed here will lead to a better understanding of why these injuries occur and how they can be prevented.

A sketch of a typical three–layered protective clothing fabric ensemble (turn-out coat) used by fire fighters is shown in Fig. 3.1. This geometry is identical to the experimental test apparatus discussed in the previous section. Because it is both an appropriate first modeling step and consistent with the experimental test apparatus a planar geometry is assumed. A further simplification is made by assuming heat transfer through the planar system is one-dimensional.

Heat transfer upon and within the material layers of the garment involves the processes of conduction, convection and thermal radiation. The relevance of each of these processes depends on local conditions. For example, convective heat transfer is assumed to occur only on the outside boundaries of the clothing

ensemble and therefore enters through the boundary conditions of the model. In one-dimension the equation governing the conservation of energy is:

$$\rho c_p \frac{\partial T}{\partial t} = -\frac{\partial q_{CD}}{\partial x} - \frac{\partial q_R}{\partial x} + g, \tag{3.1}$$

with fluxes

$$q_{CD} = -k\frac{\partial T}{\partial x}, \quad \text{conduction (Fourier law)}, \tag{3.2}$$

$$q_R, \quad \text{radiation flux (see Sec. 3.1)}. \tag{3.3}$$

Eq. (3.1) is solved within each gas or solid region of the garment. Both an initial condition and boundary conditions are required. Care must be taken in the discretization of Eq. (3.1) to ensure that the fluxes are continuous across interfaces (see Sec. 4). To obtain the temperature distribution throughout the protective clothing ensemble both the energy equation (3.1) and the radiative heat transfer equation (in some approximation) must be solved. The thermal radiation model is developed next.

3.1 Thermal Radiation Model

The radiative transfer equation for the spectral intensity, I_λ, in the absence of scattering and assuming thermodynamic equilibrium (Kirchoff's law is valid) is

$$\frac{1}{\kappa_\lambda}\frac{dI_\lambda(s,\theta,\phi)}{ds} + I_\lambda(s,\theta,\phi) = I_{b,\lambda}[T(s)], \tag{3.4}$$

where s is the path length of the radiation beam in the $\hat{\underline{\Omega}}$ direction; θ and ϕ are the polar and azimuthal angles locating the beam of radiation in a spherical coordinate system; $I_{b,\lambda}$ is the blackbody spectral intensity; T is the temperature. In general s depends on three space variables. In the context of the one-dimensional model used here (see Fig. 3.1) the intensity is independent of the azimuthal direction and points in the $\theta = 0$ or π directions (forward or backward) only. Thus, $\theta = 0$ corresponds to the direction of increasing x and

$$\frac{d}{ds} = \frac{\partial}{\partial x}\frac{dx}{ds} = \beta\frac{\partial}{\partial x}, \qquad \beta \equiv \cos\theta = 1, -1 \tag{3.5}$$

This motivates the splitting of the intensity into forward (positive x direction) and backward components, I^+ and I^- [15]:

$$I_\lambda = I_\lambda(x,\hat{\underline{\Omega}}) = I_\lambda^+(x,\hat{\underline{\Omega}}) + I_\lambda^-(x,\hat{\underline{\Omega}}) = I_\lambda^+(x)\delta(\beta-1) + I_\lambda^-(x)\delta(1+\beta). \tag{3.6}$$

To simplify the notation, when variables are spectrally dependent the λ subscript is present only on the left–hand–side of the equations to follow. Equation (3.4) is solved for a material layer (air layers are assumed to be nonparticipating) for both the backward and forward components of the spectral intensity. This scenario is depicted in Fig. 3.2 for an arbitrary material layer l.

The solution of Eq. (3.4) is

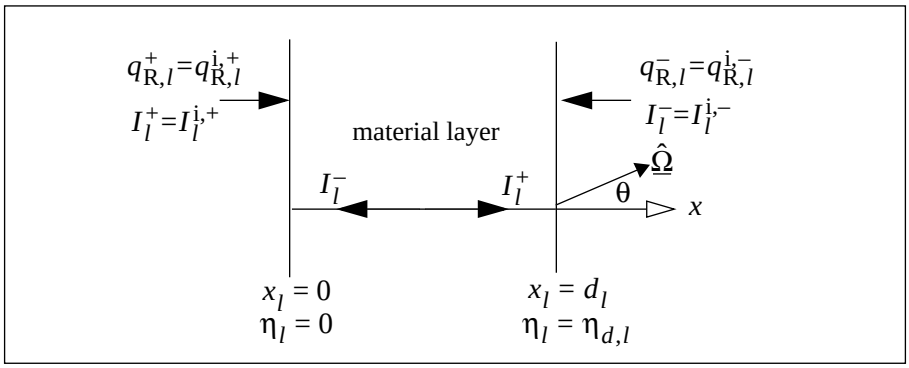

FIGURE 3.2: Geometry for solution of one-dimensional radiative transfer equation in an arbitrary material layer *l*.

$$I^+_\lambda(x) = I^{i,+}e^{-\eta} + \int_0^\eta I_b e^{-(\eta-\eta')}d\eta',$$
$$I^-_\lambda(x) = I^{i,-}e^{-(\eta_d-\eta)} + \int_\eta^{\eta_d} I_b e^{-(\eta'-\eta)}d\eta', \tag{3.7}$$

where

$$\eta_\lambda = \int_0^x \kappa dx', \tag{3.8}$$

is the nondimensional spectral absorption length. From the spectral intensities in Eq. (3.7) the spectral radiative flux can be determined

$$q_{R,\lambda} = \int_{4\pi} \Omega I(s,\hat{\Omega})d\Omega = q^+_{R,\lambda} + q^-_{R,\lambda}$$
$$= \int_0^{2\pi}\int_0^1 I^+(x,\beta)\beta d\beta d\phi + \int_0^{2\pi}\int_{-1}^0 I^-(x,\beta)\beta d\beta d\phi. \tag{3.9}$$

Only the net flux, which is found by integrating Eq. (3.7) over all wavelengths, is considered in the model

$$q^+_R(\eta) = q^{i,+}_R e^{-\eta} + \sigma\int_0^\eta T^4(\eta')e^{-(\eta-\eta')}d\eta',$$
$$q^-_R(\eta) = q^{i,-}_R e^{-(\eta_d-\eta)} - \sigma\int_\eta^{\eta_d} T^4(\eta')e^{-(\eta'-\eta)}d\eta', \tag{3.10}$$

where, $q^{i,-}_R \le 0$, the backward flux incident on the $x = d$ material boundary in non-positive. Note that spectral dependence of the fluxes can be added to the model in a straightforward way. The first terms on the right-hand-side of Eq. (3.10) are the contribution to the flux from radiation entering the boundaries. The second terms are the contribution of emission along the path length of integration (self emission).

In the current model, the major radiative fluxes incident on the boundaries of a material layer ($q^{i,+}_R$, $q^{i,-}_R$) are assumed to be due to:

1. the external incident heat flux on the outer garment layer. This contributes to the forward incident fluxes and the backward incident fluxes on the inner gas/solid boundaries if reflection occurs.
2. interlayer (across air layers) radiative flux and its reflection. This occurs when the material surfaces bounding the air layers have different temperatures and contributes to both the forward and backward incident flux.

With regard to 1, only the backward reflection of radiation due to the external flux is calculated. Note that since the radiative transfer equation is linear, the separate contributions to the forward or backward boundary fluxes for a particular boundary can be obtained and then added.

It is commonly assumed that, within a material, the contribution to the radiative flux from self emission is much smaller than that due to the absorption of the externally incident flux [i.e., terms containing I_b in Eq. (3.7) are neglected]. Under this assumption the net flux within material layer l from Eqs. (3.9) and (3.10) is (Beer-Lambert law)

$$q_{R,\,l} = q^{+}_{R\,,\,l} + q^{-}_{R,\,l} = q^{i,+}_{R,\,l} e^{-\eta_l} + q^{i,-}_{R,\,l} e^{\eta_l - \eta_{d,\,l}} \ . \tag{3.11}$$

Here $q^{i,+}_{R,l}$ and $q^{i,-}_{R,l}$ are the fluxes incident on the left and right side, respectively, of material layer l and η_l is the optical length from the left boundary of layer l (see Fig. 3.2).

The absorptivity of a fabric layer, α, is related to its transmissivity, τ, and reflectivity, r, through

$$\alpha + r + \tau = 1 \ . \tag{3.12}$$

The absorption coefficient is assumed to be constant within a material layer. This means that it can be determined from the transmissivity and reflectivity of the fabric layer. Define q_{in} to be the radiative flux on the left-hand-side surface of fabric layer l. From Eq. (3.11) the transmissivity of the fabric layer is

$$\tau_l = \frac{q^{+}_{R\,,\,l}(\eta_{d,\,l})}{q_{in}} = \frac{(1 - r_l) q_{in} e^{-\kappa_l d_l}}{q_{in}} \ . \tag{3.13}$$

This equation gives the absorption coefficient for material layer l:

$$\kappa_l = \frac{1}{d_l} \ln\left(\frac{1 - r_l}{\tau_l}\right) . \tag{3.14}$$

3.2 Radiation fluxes incident on material boundaries

As discussed above it is assumed that the radiant flux on a material boundary is from two sources: the external radiation source (q_e) and the interlayer flux (denoted, for example, $q_{1\text{-}2}$ for fabric layers 1 and 2). These fluxes are depicted in Fig. 3.3. The contributions to the incident boundary flux due to the external flux, $q^{i,+/-}_{e,l}$, are as follows. (Note, the backward component is due to reflection only from the next material layer).

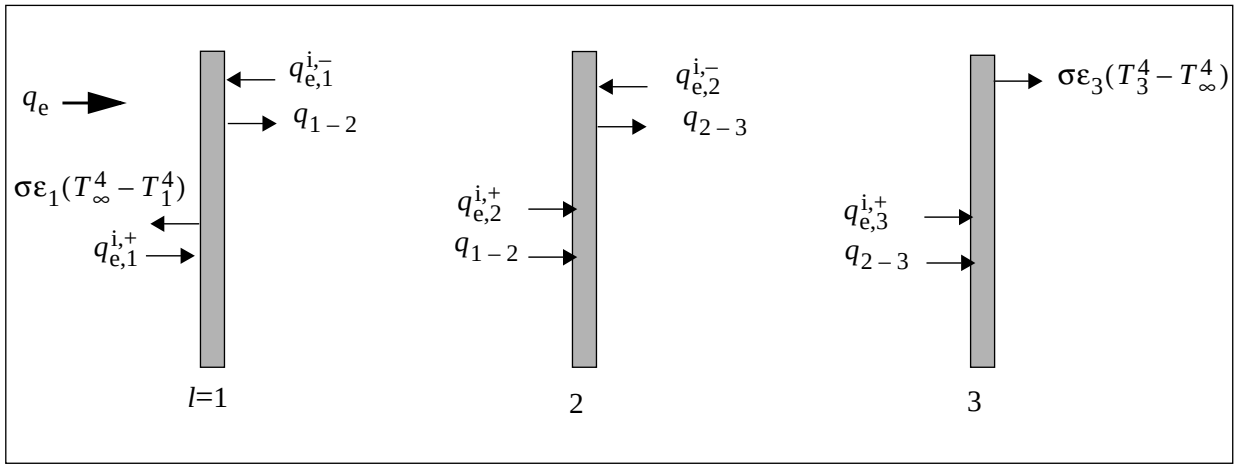

FIGURE 3.3: Radiative fluxes included in the model which are incident on material boundaries in a three layer clothing assembly surrounded by ambient air of temperature T_∞.

Fabric Layer 1

$$q^{i,+}_{e,1} = q_e(1-r_1)$$
$$q^{i,-}_{e,1} = -r_2 q^{+}_{R,1}(\eta_{d,1}) = -q_e r_2(1-r_1)e^{-\eta_{d,1}} \tag{3.15}$$

Fabric Layer 2

$$q^{i,+}_{e,2} = (1-r_2)q^{+}_{R,1}(\eta_{d,1}) = q_e(1-r_2)(1-r_1)e^{-\eta_{d,1}}$$
$$q^{i,-}_{e,2} = -r_3 q^{+}_{R,2}(\eta_{d,2}) = -q_e r_3(1-r_2)(1-r_1)e^{-(\eta_{d,1}+\eta_{d,2})} \tag{3.16}$$

Fabric Layer 3

$$q^{i,+}_{e,3} = (1-r_3)q^{+}_{R,2}(\eta_{d,2}) = q_e(1-r_3)(1-r_2)(1-r_1)e^{-(\eta_{d,1}+\eta_{d,2})} \tag{3.17}$$
$$q^{i,-}_{e,3} = 0$$

Note that all boundary fluxes are in terms of the radiative properties of the material layers and the external flux.

The net interlayer radiative flux is computed by using the result for plane parallel plates with isotropic scattering, diffusively reflecting boundaries separated by nonparticipating air (optically thin, $\kappa_a d_a \ll 1$). With this assumption q_{1-2} from Eq. (3.9) for intensities integrated over all wavelengths ([15], p. 315) is

$$q_{1-2} = \frac{\sigma(\varepsilon_1 T_1^4 + r_1\varepsilon_2 T_2^4)}{1-r_1 r_2} - \frac{\sigma(\varepsilon_2 T_2^4 + r_2\varepsilon_1 T_1^4)}{1-r_1 r_2}\,. \tag{3.18}$$

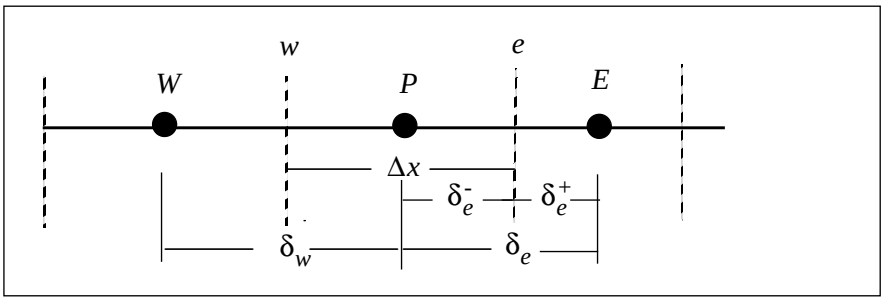

FIGURE 4.1: One-dimensional control volume.

Thus, the net incident flux on a the left side of material layer l=2 (for example) is the sum of the two contributions

$$q_{R,2}^{i,+} = q_{e,2}^{i,+} + q_{1-2}. \tag{3.19}$$

This incident flux in used in Eq. (3.11).

4 Numerical model

A control volume approach was used to derive the finite difference form of Eq. (3.1). This method of discretization ensures local energy conservation and requires approximation of only first order derivatives (rather than higher order). A second order Runge-Kutta scheme was used for time stepping. The stability characteristics of Runge-Kutta are not as attractive as an implicit scheme such as Crank–Nicholson —leading to a more computationally expensive algorithm. However, the Runge-Kutta scheme was chosen at this stage of the model's development because it allows for a more simple and direct incorporation of a temperature dependent conductivity.

4.1 Discretization of model equation

Material interfaces occur at control volume interfaces. An arbitrary control volume surrounding grid point P (at the center of the control volume) is depicted in Fig. 4.1.

Control volume faces are marked by dashed lines; the left face is denoted by w and the right face by e. Grid points to the left and right of P are denoted by W and E, respectively. Note that in general the control volumes are not of constant size [i.e., $\delta_w \neq \delta_e \neq \Delta x = (\delta_w + \delta_e)/2$]. Integrating Eq. (3.1) over the control volume centered about P gives

$$\int_w^e c_p \rho \frac{\partial T}{\partial t} dx dA = k \frac{\partial T}{\partial x}\bigg|_w^e dA - q_R\big|_w^e dA + \int_w^e g dx dA, \tag{4.1}$$

where dA is a constant and the conductivity, k, can depend on temperature. Note that the equation is nonlinear when the conductivity k depends on temperature. The approach for each term in Eq. (4.1) is discussed briefly below:

1. It is assumed that the rate at which energy is stored in the control volume, $c_p \rho \partial T / \partial t$, is constant throughout the volume. The validity of this assumption will improve as the size of the control volume decreases.
2. The first order derivatives in the conduction flux term are obtained by assuming T varies linearly within a control volume. Care must taken to ensure that the flux $-q_{CD} = k \partial T / \partial x$ is continuous at cell interfaces. This is achieved by determining an effective conductivity coefficient, k^*, at the cell interface as follows. The heat conduction flux at interface e in Fig. 4.1 is expressed as

$$k \frac{\partial T}{\partial x}\bigg|^{e} = k_E \frac{(T_E - T_e)}{\delta_e^+} = k_P \frac{(T_e - T_P)}{\delta_e^-} . \tag{4.2}$$

   Note that the conductivity is assumed to be constant within a control volume. Solving for T_e from the second and third terms and substituting the result into the second term gives

$$k \frac{\partial T}{\partial x}\bigg|^{e} = k^* (T_E - T_P), \quad 1/k^* = \frac{\delta_e^-}{k_P} + \frac{\delta_e^+}{k_E} . \tag{4.3}$$

   A similar method is used for fluxes at the gas/solid boundaries (Sec. 4.2).
3. The radiative flux is obtained from Eq. (3.11).
4. Internal heat generation may occur if, for example, a melting fabric solidifies; heat losses may occur by fabric pyrolysis or melting. These processes are not considered at this stage of the model ($g \equiv 0$).

With the above assumptions the discretized energy equation becomes

$$\overline{c_p \rho \frac{\partial T}{\partial t}}\bigg|^{P} \Delta x dA = k \frac{\partial T}{\partial x}\bigg|_{w}^{e} dA - q_R\big|_{w}^{e} dA . \tag{4.4}$$

where the overbar indicates the quantity is a cell average. This equation is solved for each material layer and air gap. Boundary conditions for the conductive and radiation fluxes are needed on all internal gas/solid boundaries. Convective losses must also be included at the two outer gas/solid boundaries. These boundary fluxes are considered next.

4.2 Boundary conditions

The external radiative flux (possibly time varying) on the outer surface of the garment is specified, as are the ambient air temperatures on each side of the fabric assembly. Continuity of the heat fluxes across the gas/solid boundaries must be enforced to conserve energy. There are two types of gas/solid boundaries distinguished according to whether or not convective heat transfer is present. The two outer boundaries of garment involve convective heat transfer and the associated surface heat transfer coefficient, h_c (Fig. 3.1). The thickness of the air gaps between fabric layers (~ 1 mm) is small enough to assume that no velocity boundary layer develops and heat transfer is by conduction.

The situation for the outer surface of the garment facing the external radiation source is depicted in Fig. 4.2. The solid and gas cells have mean temperatures T_S and T_G. The temperatures on the solid and gas

sides of the surface layer are T_s and T_g, respectively. Continuity of the fluxes across the surface layer requires (using the cell spacing of Fig. 4.1)

$$-q(x_\Gamma) = \frac{k_S}{\delta_e^+}(T_S - T_s) = h_c(T_s - T_g) = \frac{k_G}{\delta_e^-}(T_g - T_G) \ . \tag{4.5}$$

Solving for the surface layer temperatures T_s, T_g and substituting the result into Eq. (4.5) gives

$$-q(x_\Gamma) = k_\Gamma(T_S - T_G) \ , \qquad \frac{1}{k_\Gamma} = \frac{\delta_e^-}{k_S} + \frac{\delta_e^+}{k_G} + \frac{1}{h_c} \ . \tag{4.6}$$

The surface heat transfer coefficient, h_c, was obtained from the Nusselt number through empirical correlations of free convection on a vertical plate [16]

$$h_c = \mathrm{Nu}\frac{k_G}{L} \ . \tag{4.7}$$

Correlations appropriate for both laminar and turbulent flow were used depending on the magnitude of the Rayleigh number. For laminar flow the correlation is

$$\mathrm{Nu} = 0.68 + \frac{0.67\ \mathrm{Ra}^{1/4}}{(1 + [0.492/\mathrm{Pr}]^{9/16})^{4/9}}, \quad 10^{-1} < \mathrm{Ra} < 10^9 \ . \tag{4.8}$$

When $\mathrm{Ra} > 10^9$ the following correlation for turbulent flow was used

$$\mathrm{Nu}^{1/2} = 0.825 + \frac{0.387\ \mathrm{Ra}^{1/4}}{(1 + [0.492/\mathrm{Pr}]^{9/16})^{8/27}} \ . \tag{4.9}$$

The temperature dependent values of density and viscosity of air used in Nusselt number were determined at $(T_G + T_\infty)/2$. A constant value of the Prandtl number was used, Pr = 0.7. Equation (4.6) defined the conductive heat flux in Eq. (4.4) at the outer boundaries. Radiative fluxes on the boundaries were obtained from expressions developed in Sec. 3.2.

Similarly, at the gas/solid boundaries of the internal material layer 2, for which no thermal boundary layer exists, continuity of the conductive heat fluxes across the interface is ensured by using

$$-q(x_\Gamma) = k_\Gamma(T_S - T_G) \ , \qquad \frac{1}{k_\Gamma} = \frac{\delta_e^-}{k_S} + \frac{\delta_e^+}{k_G} \ . \tag{4.10}$$

5 Turnout Coat Characteristics

As depicted in Fig. 3.1 a typical turn-out coat consists of three fabric layers: the shell (outermost layer, farthest from skin), the moisture barrier and the thermal liner. Various physical characteristics of the fabrics under normal loft are listed in Table 1. To perform a simulation the thickness, density, conductivity, specific heat and the optical properties of transmissivity and reflectivity were needed for each fabric layer. All the fabrics were clean (unused). Thickness was measured with a micrometer. For a given fabric, three different samples were measured 12 times giving a total of 36 independent measurements. Density was

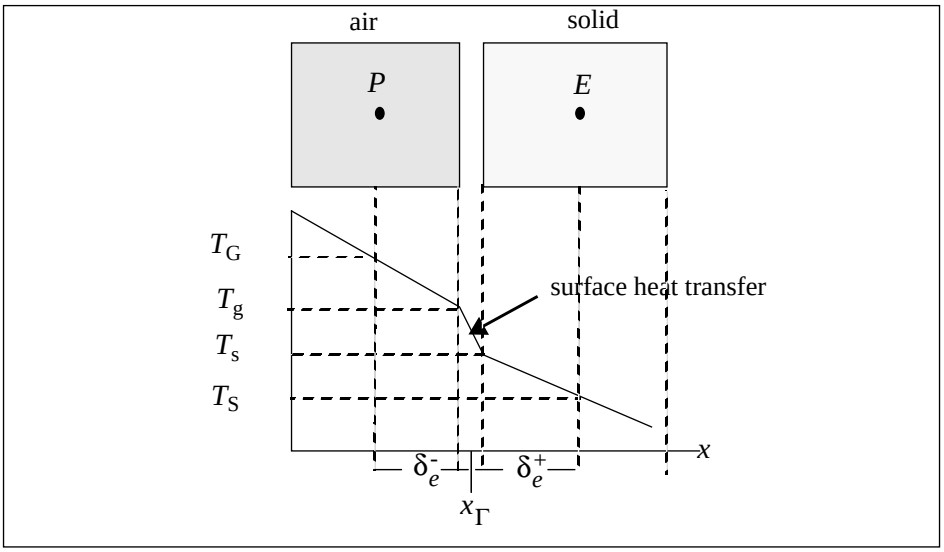

FIGURE 4.2: Solid/gas interface at outer surface of garment.

TABLE 1: Physical characteristics of fabric layers (at 20 ˚C).

Fabric Characteristic	**Shell**	**Moisture Barrier**	**Thermal Liner**
Thickness (cm)	0.082 ± 0.007	0.055 ± 0.005	0.35 ± 0.04
specific mass (g/m^2)	254	440	240
density (g/cm^3)	0.31 ± 0.024	0.8 ± 0.06	0.072 ± 0.007
conductivity (W/cm·C)	4.7×10^{-4} [1]	1.2×10^{-4} (soft rubber, [16])	3.8×10^{-4} (glass wool, [16])
specific heat (J/g·C)	1.3 [1]	2.01 (soft rubber, [16])	0.7 (glass wool, [16])
transmissivity (see text)	0.044	0.005	0.0012
reflectivity (see text)	0.09	0.017	0.002
color	black	white	yellow

obtained in two ways when possible: from the measured thickness, area and mass or from the measured thickness and area density from the manufacturer (when available). In the turnout coat considered here the shell material is Nomex® IIIA, the moisture barrier is neoprene, and the thermal liner is Aralite®.[1] The conductivity, specific heat and optical properties of the fabrics were not measured. When possible, these property values were obtained from the literature (references are cited in Table 1). When no values could be found those for similar fabrics were used until measured values can be obtained. For example, the specific heats of soft rubber and glass wool were used for the moisture barrier and thermal layer, respectively. Table 1 lists the material properties used in the simulations reported here.

1. Certain commercial equipment, instruments, or materials are identified in this paper in order to adequately specify the materials used and the experimental procedure. Such identification does not imply recommendation or endorsement by the National Institute of Standards and Technology, nor does it imply that the materials or equipment identified are necessarily the best available for the purpose.

As mentioned above, the model used the total or spectrally integrated value of the transmissivity and reflectivity. These were calculated from their spectrally dependent values. For example, in the case of the shell layer,

$$\tau_1 = \frac{\int_0^\infty E_{b,\lambda}\tau_{\lambda,1}\,d\lambda}{\int_0^\infty E_{b,\lambda}\,d\lambda}, \qquad r_1 = \frac{\int_0^\infty E_{b,\lambda}r_{\lambda,1}\,d\lambda}{\int_0^\infty E_{b,\lambda}\,d\lambda}. \tag{5.1}$$

The spectral energy distribution from the central region of a gas-fired radiant panel approximates that of a blackbody source at 943 K [17] which was used for $E_{b,\lambda}$ in Eq. (5.1).

Bamford and Boydell [10] use the specific mass of the fabric to determine values of τ_λ and r_λ for four wavelength bands (visible, 0.4 μm - 0.7 μm; 0.7 μm - 2.5 μm; 2.5 μm - 5 μm; and > 5 μm). These band averaged transmissivities can then be used in Eq. (5.1). It should be noted that the method used by Bamford and Boydell [10] to obtain τ and r is based on a compilation of optical property measurements [4]. Common clothing fabrics (cotton, polyester, acetate, acrylic and wool) were measured. More specialized fabrics used in fire fighter protective clothing, such as Nomex® were not considered. Thus, the accuracy of the optical properties obtained via Bamford and Boydell should be viewed with some caution. For example, Fig. 6 in Quintiere [18] shows that twill cottons and aromatic polyamide (generic Nomex®) of the same specific mass have markedly different spectral behavior (in the wavelength range 0.7 μm - 2.5 μm). Even when the total transmissivity for a given fabric is measured different values are reported. For a shell fabric with a specific mass of approximately 140 g/m^2 reported values are: $\tau = 0.11$ for aromatic polyamide with a 1000 K blackbody source [18]; $\tau = 0.17$ for Nomex with a 1250 K blackbody source [5]; the method used by Bamford and Boydell gives $\tau = 0.08$ with a 1100 K blackbody source. Similarly, the total reflectivities for the cases just considered are $r = 0.24$ [18], $r = 0.26$ [5] and $r = 0.09$ from Bamford and Boydell. As with the transmissivity, the reflectivity of Nomex® obtained following Bamford and Boydell is lower than those in the literature. In fact, Quintiere found that, irrespective of color or specific mass, $r \approx 0.22$ for a number of commonly used cotton-based and aromatic polyamide shell fabrics (1000 K blackbody source temperature).

It is clear from the variation of the optical property values found in the literature that these properties need to be measured for the specific fabric to be simulated. However, pending these measurements, base case values of the spectral transmissivity and reflectivity for each fabric layer were determined using the method of Bamford and Boydell. This was done because no optical property information was found on neoprene or Aralite® and the method used by Bamford and Boydell only requires the specific mass. Figure 5.3 shows the normalized spectral blackbody emissive power and spectral transmissivity from which the total transmissivity was calculated [Eq. (5.1)] for the Nomex® IIIA shell fabric used in this study. The total reflectivity of the shell was computed in a similar manner. The moisture barrier was subjected to the gas-fired panel's radiative spectrum as transmitted in modified form through the shell. From the definition of the spectral transmissivity [16] the spectral emissive power incident on the moisture barrier is

$$E_{\lambda,2} = \tau_{\lambda,1}E_{b,\lambda}. \tag{5.2}$$

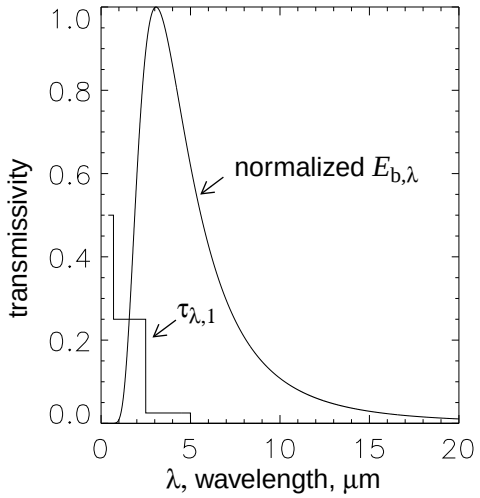

FIGURE 5.3: Normalized spectral blackbody emissive power versus wavelength which approximates the emission of the gas-fired radiative panel (blackbody source temperature of 943 K). Also shown is the assumed spectral transmissivity from Bamford and Boydell [10] for Nomex® IIIA of specific mass 254 g/m^2.

Equation (5.2) along with the spectral transmissivity of the moisture barrier were used in Eq. (5.1) to compute the total transmissivity of the moisture barrier. The total reflectivity of the moisture barrier was computed in a similar way. The base case values of the optical properties are given in Table 1. Both air gaps were assumed to be 1 mm thick. The specific heat of air, which is weakly dependent on temperature, was set equal to its value at 20 C (1.006 J/g·C). The temperature dependence of the conductivity and density of air were fitted by polynomials.

6 Model Results

6.1 Verification

It is useful to compare the results of the numerical method to exact solutions of simplified problems. The performance of the numerical method can then be tested and the grid resolution required for suitably accurate results can be determined. To test the model for the case of two materials with different properties the exact solution to the following problem was used:

$$U(x,t) = T(x,t) - T(x,0),$$

$$\frac{\partial U_1}{\partial t} = D_1 \frac{\partial^2 U_1}{\partial x^2}, \quad 0 \le x \le x_\Gamma ; \qquad \frac{\partial U_2}{\partial t} = D_2 \frac{\partial^2 U_2}{\partial x^2}, \quad x_\Gamma \le x \tag{6.1}$$

$$-k_1 \frac{\partial U_1(0,t)}{\partial x} = H \quad \text{for } 0 \le t.$$

Equation (6.1) along with continuity conditions of both U and its flux at the interface two different materials ($x = x_\Gamma$) governs the change in temperature due to a constant flux H on the $x = 0$ boundary. The solution

has been found using Laplace transforms ([19] with corrections in [6]). The prescribed constant boundary flux H can be viewed as the net flux due to radiation, conduction and convection at the boundary. Time dependent radiative and convective heat losses at the boundary, which increase with temperature, are not present. The exact solution to Eq. 6.1 is

$$\begin{aligned} U_1 = \frac{H}{k_1}\Bigg(\Bigg\{ & 2\sqrt{\frac{D_1 t}{\pi}}e^{-\frac{x^2}{4D_1 t}} - x\left(1-\operatorname{erf}\frac{x}{2\sqrt{D_1 t}}\right)\Bigg\} \\ & -\frac{1}{\gamma}\sum_{n=0}^{\infty}\left(\frac{1}{\gamma}\right)^n\Bigg[2\sqrt{\frac{D_1 t}{\pi}}\left(e^{-\frac{a^2}{4D_1 t}}+e^{-\frac{b^2}{4D_1 t}}\right) - a\left\{1-\operatorname{erf}\left(\frac{a}{2\sqrt{D_1 t}}\right)\right\} \\ & + b\left\{1-\operatorname{erf}\left(\frac{-b}{2\sqrt{D_1 t}}\right)\right\}\Bigg]\Bigg) \end{aligned} \tag{6.2}$$

$$U_2 = \frac{2H\alpha\sqrt{D_1}}{x_\Gamma}\sum_{n=0}^{\infty}\left(-\frac{1}{\gamma}\right)^n\left\{2\sqrt{\frac{D_2 t}{\pi}}e^{-\frac{c^2}{4D_2 t}} - c\left(1-\operatorname{erf}\frac{c}{2\sqrt{D_2 t}}\right)\right\} \tag{6.3}$$

and at the material interface, $x = x_\Gamma$,

$$\begin{aligned} U(x_\Gamma, t) = \frac{H}{k_1}\sum_{n=0}^{\infty}\left(-\frac{1}{\gamma}\right)^n\left(1-\frac{1}{\gamma}\right)\Bigg[& 2\sqrt{\frac{D_1 t}{\pi}}e^{-\left(\frac{x_\Gamma(2n+1)}{2\sqrt{D_1 t}}\right)^2} \\ & -x_\Gamma(2n+1)\left(1-\operatorname{erf}\frac{x_\Gamma(2n+1)}{2\sqrt{D_1 t}}\right)\Bigg] \end{aligned} \tag{6.4}$$

where

$$\gamma = \frac{k_2 c_{p,2}\rho_2 + \sqrt{k_1 c_{p,1}\rho_1 k_2 c_{p,2}\rho_2}}{k_2 c_{p,2}\rho_2 - \sqrt{k_1 c_{p,1}\rho_1 k_2 c_{p,2}\rho_2}}, \qquad \alpha = (k_2\sqrt{D_1} - k_1\sqrt{D_2})^{-1},$$

$$a = x + 2x_\Gamma(n+1), \qquad b = x - 2x_\Gamma(n+1),$$

$$c = x - x_\Gamma\{1 - \sqrt{D_2/D_1}(2n+1)\}.$$

This solution can be used to ensure that the discontinuity of the conduction coefficient at the material interface is handled properly by the numerical method. Unlike the flux due to conduction, the radiative flux in Eq. (4.4) was directly modeled. Its accuracy depends on the validity of the physical model for radiative heat transfer and on using appropriate optical properties —not on the accuracy of numerical differentiation. Thus, even though radiative absorption and emission are absent, using Eq. (6.1) does test the accuracy of the full numerical model. (There is a minor exception to this statement which will be discussed below).

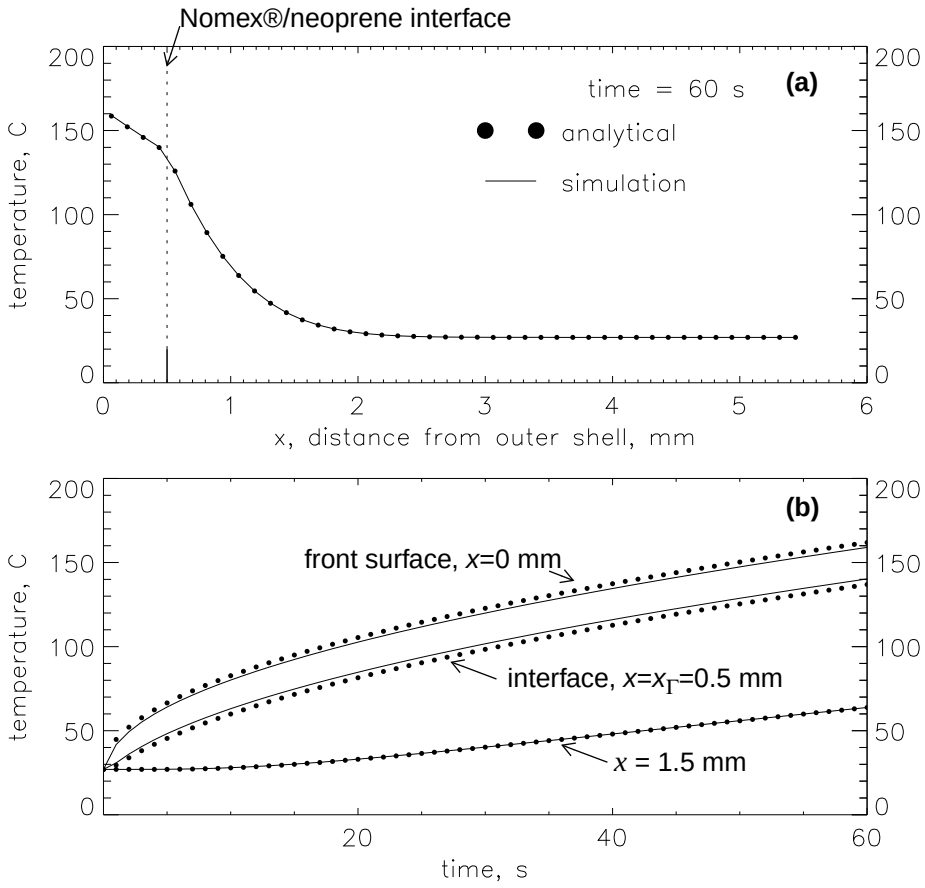

FIGURE 6.1: Temperature from the exact and numerical solution of the one-dimensional conduction equation for a two material semi-infinite solid subject to a constant heat flux.

The case of a $x_\Gamma = 0.5$ mm layer of Nomex® against a 5 mm layer of neoprene was simulated. The external flux was 0.25 W/cm^2. This flux was also used in the simulation of an experimental test apparatus case to be discussed below. Material properties from Table 1 were used. The temperature profile throughout the two material layers at $t = 60$ s is shown in Fig. 6.1(a). Temperatures from the exact solution at computational grid point locations are shown as dots. The Nomex®/neoprene interface can be seen to reside midway between the adjacent control volumes. Temperatures from the exact and numerical solutions are in excellent agreement. The temperature time histories at three locations in the fabric assembly are plotted in Fig. 6.1(b). The exact and numerical temperature are again in excellent agreement at the interior point $x = 1.5$ mm. Since numerical values of the temperature exist only at control volume centers they are not known at material interfaces. This is the source of the disagreement ($|T_{\text{exact}} - T_{\text{model}}| \leq 3$ ˚C at $t = 60$ s) between the numerical and exact temperatures at $x = 0$ mm and $x = x_\Gamma = 0.5$ mm in Fig. 6.1(b). Some error will therefore be introduced when computing the interlayer radiative fluxes [Eq. (3.18)] and the radiative flux to the ambient surroundings. However, the difference between the exact and numerical solution is sufficiently small that this error will be negligible. The results above show that the numerical procedure accurately computed heat transfer through the interface between two fabrics commonly used in turnout coats.

6.2 Turnout Coat Simulation

A turnout coat assembly with material characteristics listed in Table 1 was subjected to thermal radiation from a gas-fired radiation panel as discussed in Sec. 2. The total radiative flux on the shell of the turnout coat was q_e = 0.25 W/cm^2. This flux is characterstic of the pre-flashover fire environment in which structural fire fighters typically work [21]. Thermocouples of type K and size 10 mil (0.254 mm) were sewn on the front surface of the shell (x = 0 mm), and both the inner air/fabric interface (x = 3.4 mm) and the outer fabric/air interface (x = 6.9 mm, back surface of garment) of the thermal liner. The turnout coat material was subject to radiation from the gas panel for 300 s after which a radiation shield was placed between the coat and the gas-fired panel. A cool down period of approximately 10 min followed. The turnout coat sample was then removed from the experimental test apparatus. Ten such tests, separated by approximately 10 min, were completed. From these ten tests the mean and standard deviation of the temperature at each thermocouple were computed. The ambient mean temperature was found to be T_∞ = 29.3 ˚C.

On Fig. 6.2(a) the temperature time history from the simulation and experiment at the three thermocouple locations are plotted. The temperature difference between the simulation and the experiment (mean values) are plotted versus time in Fig. 6.2(b). Heat transfer through the turnout coat reaches a steady state after approximately 100 s. Figure 6.3 shows the simulated and experimental temperatures versus distance into the turnout coat at three different times, t = 0 s, 200 s (during steady state), 400 s. Vertical dotted lines mark the air/solid interfaces. Mean temperatures from the thermocouples (at x = 0 mm, x = 3.4 mm, 6.9 mm) are plotted as black circles with error bars extending one standard deviation above and below. Simulated temperatures are plotted as solid lines. During the steady state period the simulated shell temperature is approximately 15 ˚C higher than experimentally obtained temperatures. The largest error in the model occurred in the prediction of temperatures on the outer shell surface during the first half of the experiment before the flux from the radiant panel was blocked. A probable source of this error is the approximate manner by which the transmissivity and reflectivity values have obtained. A majority of the incident radiant heat flux is absorbed by the shell. Thus, it is especially important in the case of the shell to use accurate values for the transmissivity and reflectivity. After the radiant panel is blocked, the material properties of the fabric layers (conductivity, specific heat and density) play a more important role, as does convective heat loss from the boundaries. Note that during the cool down period the simulated and experimental temperatures for the shell are in better agreement. The simulated temperatures in the interior of the garment were within approximately 5 ˚C of the mean experimental temperature.

Based on these results it appears that the model could be used to predict the thermal performance of fire fighters' protective clothing (at least under heat flux conditions consistent with the model assumptions). More data from experiments using materials for which the optical and thermal properties of the materials are known is required before the accuracy of the model can be conclusively measured. Measurements are currently being made of material properties necessary for modeling the thermal behavior of fabrics and fabric assemblies commonly used in fire fighter gear.

The net radiative flux from the simulation at both the front surface of the shell and the back surface of the thermal liner are plotted versus time in Fig. 6.2(c). During the time interval t = 0 s to 300 s the flux on the front surface was reduced from 0.25 W/cm^2 to 0.14 W/cm^2 by reflection and radiation to the surround-

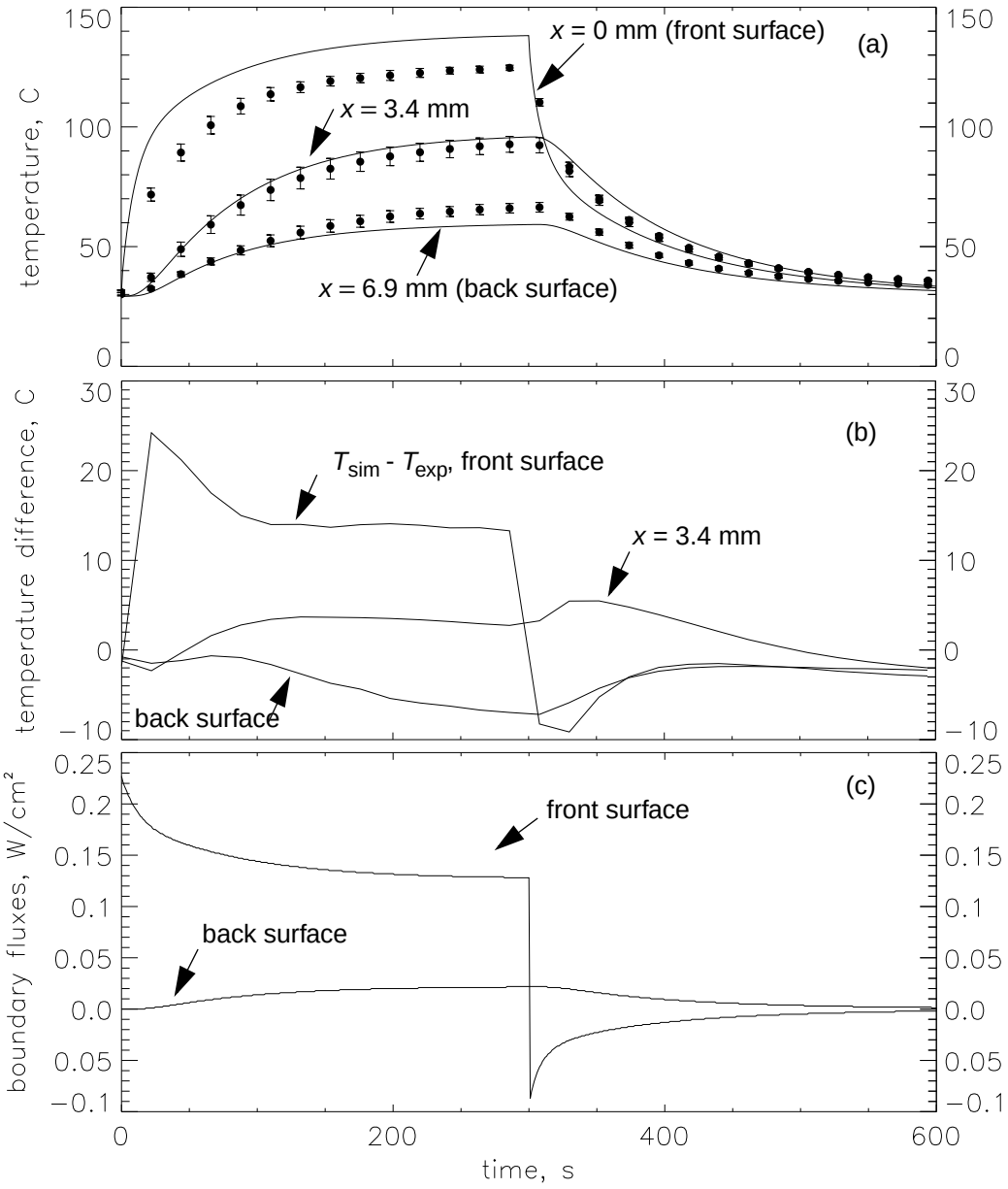

FIGURE 6.2: (a) Simulation time history (lines) and mean experimental temperature (filled circles) with +/- standard deviation spread for the Nomex®/neoprene/Aralite® assembly. Results at the three thermocouple locations (x = 0 mm, 3.4 mm, 6.9 mm) are shown. (b) Difference between temperatures from the simulation and experiment shown in Fig. (a) versus time. (c) Net thermal radiation flux versus time from the model, at the front (x = 0 mm) and back (x = 6.9 mm) boundaries of clothing assembly.

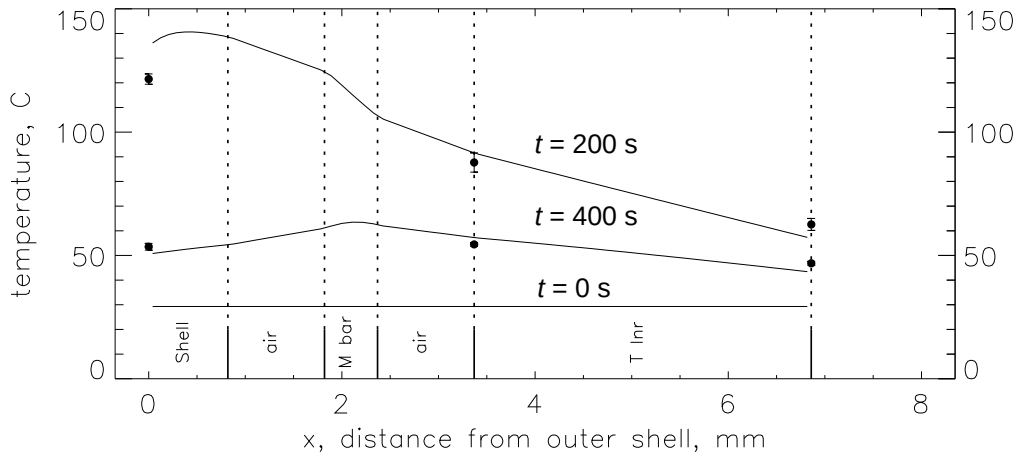

FIGURE 6.3: Profiles of simulated temperature (lines) through the Nomex®/neoprene/Aralite® assembly at three different times: t = 0 s, 200 s, 400 s. The mean temperature (filled circles) and +/- standard deviation spread from ten experimental runs are also shown at the front surface of the shell, the internal air/thermal liner interface and at the back of the assembly.

ings. After radiation from the gas-fired panel was removed at 300 s radiative cooling occurred. Note that if the ambient temperature is increased to 65 ˚C which is commonly experienced by fire fighters [21] the net radiative flux on the shell at 300 s would increase to 0.16 W/cm^2 for the same shell temperature. On the back surface the radiative flux gradually increased to a maximum of 0.025 W/cm^2 as the temperature of the thermal liner rose [Fig. 6.2(a)]. This flux was entirely due to the temperature of the thermal liner relative to the ambient temperature, T_∞, since the contribution of the external flux q_e was negligible. If the ambient temperature is increased to T_∞ = 32 ˚C (normal core skin temperature) the back surface flux decreases to 0.023 W/cm^2 for the same thermal liner temperature.

Figures. 6.2 - 6.3 show that the clothing ensemble clearly provided protection against the incident radiative flux. From the outside of the shell to the back of the thermal liner the temperature fell nearly 70 ˚C. The effects of the moisture barrier's lower thermal conductivity are apparent by the relatively steep drop in temperature in the t = 200 s temperature profile in Fig. 6.3. The steady state temperature at the back of the thermal liner reached 66 ˚C. Note that when a fire fighter wears a turnout coat the apparent temperature in the air gap between the turnout coat and the fire fighter will rise due to an increased relative humidity. For the incident flux and protective clothing assembly considered here heat transfer to the fire fighter would occur predominantly through conduction rather than radiation from the thermal liner.

7 Summary and Conclusions

The goal of this project at NIST is to improve fire fighter safety through a better understanding of heat transfer in the protective garments worn by fire fighters. Both experimental and modeling approaches were used. This paper focuses on the formulation of the first stage in a heat transfer model suitable for predicting

temperature and heat flux in fire fighter protective clothing. For this reason model results were compared to only one experimental case (q_e = 0.25 W/cm^2, typical of pre-flashover fires) with one commonly used three-layer protective clothing assembly. Model predictions of the temperature agreed very well with experimental temperature for the interior layers (within 5 ˚C). Temperature predictions on the outer shell were up to 24 ˚C higher than experimentally measured values (while the external radiative flux was present). Error in the estimates of transmissivity and reflectivity was most likely the source of modeling error in the shell temperatures. No measurements of these optical properties for any of the fabrics were available. Instead, these property values were based on previous work in the literature. NIST is currently developing a database of material properties for fabrics and materials commonly used in fire fighter protective gear. Further application and testing of the model using other fabric assemblies and heat flux environments is needed to verify the model.

The model was designed, as much as possible, to accommodate the variable thermal environments in which a fire fighter works. While this capability was not shown here, the incident radiative heat flux, fabric thickness, air gap thickness or the presence or absence of an air gap can be varied dynamically during the simulation.

At this stage, the model is restricted to dry fabrics and temperature and flux levels which are sufficiently low that no thermal degradation of the fabric occurs. Further developments should include moisture effects and a multiple-layer, variable property skin mode. Estimations of burn injury risk would then be possible.

8 Acknowledgments

Appreciation is extended to Mr. Robert T. McCarthy of the United States Fire Administration for assistance provided during discussions related to fire fighter burn injuries and protective clothing performance. The United States Fire Administration provided funding for the National Institute of Standards and Technology, Building and Fire Research Laboratory to study issues related to fire fighter's station/work uniforms and protective clothing. Mr. William Twilley of the Building and Fire Research Laboratory assisted in the development of the experimental test apparatus.

9 References

1. Torvi, D.A. (1997), "Heat Transfer in Thin Fibrous Materials Under High Heat Flux Conditions," PhD Thesis, Mechanical Eng. Dept., University of Alberta, Calgary, Alberta.
2. Chen, N.Y. (1959), "Transient Heat and Moisture Transfer Through Thermally Irradiated Cloth," PhD Thesis, Massachusetts Institute of Technology, Cambridge, MA.
3. Backer, S. *et. al.* (1976)"Textile Fabric Flammability," The MIT Press, Cambridge, MA.
4. Wulff, W., Zuber, N. *et al.* (1972) "Study of Hazards from Burning Apparel and the Relation of Hazards to Test Methods," Second Final Report: Georgia Inst. Tech., NTIS: COM-73-10956.
5. Morse, H.L., Green, K.A., Thompson, J.G., Moyer, C.B. and Clark, K.J. (1972) "Analysis of the Thermal Response of Protective Fabrics," *Technical Report*, Acurex Corp., Mountain View CA

6. Stoll, A.M., Chianta, M.A. and Munroe, L.R. (1964), "Flame-Contact Studies," *Transactions of the ASME, Journal of Heat Transfer*, **86**, pp. 449-456.
7. Stoll, A.M. and Chianta, M.A. (1968) "Burn Protection and Prevention in Convective and Radiant Heat Transfer," *Aerospace Medicine*, **39**, pp. 1097-1100.
8. Stoll, A.M. and Chianta, M.A. (1969), "Method and Rating System for Evaluation of Thermal Protection," *Aerospace Medicine*, November, pp. 1232 - 1238.
9. American Society for Testing and Materials, (1987) "ASTM D 4108-87 Standard Test Method for Thermal Protective Performance of Materials for Clothing By Open-Flame Method," West Conshohocken, PA.
10. Bamford, G.J. and Boydell, W. (1995), "ICARUS: A Code for Burn Injury Evaluation," *Fire Technology*", **31**, (4), pp. 307-335.
11. NFPA 1971, Standard on Protective Ensemble for Structural Fire Fighting, 1997 Edition, National Fire Protection Association, Quincy, MA.
12. Krasny, J.F., Rockett, J.A. and Huang, D. (1988), "Protecting Fire Fighters Exposed in Foom Fires: Comparison of Results of Bench Scale Test for Thermal Protection and Conditions During Room Flashover, *Fire Technology*, February, National Fire Protection Association, Quincy, MA.
13. Peacock, R.D., Krasny, J.F., Rockett, J.A. and Huang, D. (1990), "Protecting Fire Fighters Exposed in Room Fires, Part 2: Performance of Turnout Coat Materials Under Actual Fire Conditions," *Fire Technology*, **26**, pp. 202-222.
14. Lawson, J.R. (1996) "Fire Fighter's Protective Clothing and Thermal Environments of Structural Fire Fighting," NISTIR 5804, National Institute of Standards and Technology, Gaithersburg, MD.
15. Özisik, M.N. (1973), "Radiative Transfer and Interactions with Conduction and Convection," John Wiley & Sons, New York
16. Ozisik, M.N. (1985) "Heat Transfer A Basic Approach," McGraw-Hill, Inc., New York, NY
17. Comeford, J.J. (1972), "The Spectral Distribution of Radiant Energy of a Gas-Fired Radiant Panel and Some Diffusion Flames," *Combustion and Flame*, **18**, pp. 125-132.
18. Quintiere, J. (1974), "Radiative Characteristics of Fire Fighter's Coat Fabrics," *Fire Technology*, **10**, pp. 153-161.
19. Griffith, M.V. and Horton, G.K. (1946) "The Transient Flow of Heat Through a Two-Layer Wall," *Proceedings of the Philosophical Society*, London, England, **56**, pp. 481-487.
20. Wu, Yung–Chi (1972), "Material Properties Criteria for Thermal Safety," *Journal of Materials*, **4**, pp. 573 - 579.
21. "Minimum Standards on Structural Fire Fighting Protective Clothing and Equipment: A Guide for Fire Service Education and Procurement," Federal Emergency Management Agency, United States Fire Administration, FA-137.